Supporting information

Microwave-Induced Structural Ordering of Resilient Nanostructured $L1_0$-FePt Catalysts for Oxygen Reduction Reaction

Robin Sandström[a], Eduardo Gracia-Espino[a], Alagappan Annamalai[a], Per O.Å. Persson[b], Ingemar Persson[b], Joakim Ekspong[a], Hamid Reza Barzegar[a], Thomas Wågberg[*,a]

[a]Department of Physics, Umeå University, Umeå 90187, Sweden

[b]Thin Film Physics Division, Department of Physics, Chemistry, and Biology (IFM), Linköping University,SE-581 83 Linköping, Sweden

*Corresponding author, E-mail: Thomas.wagberg@umu.se

Synthesis of FePt/C* and FePt/C catalysts: comments and supplementary samples

It was observed during the experiments that generally the initial microwave irradiation time in the first step (~1-5 min) only slightly influenced the electrochemical surface area and catalytic activity but was slightly higher at maximum continuous irradiation time while also had a positive impact on the ordering after the secondary MW-annealing step. Continued heating after a "pause" did however lower the Pt-area, suggesting that the FePt(X:Y)/C* samples were prepared close to optimum conditions. In the secondary step, it was generally observed that the reductive atmosphere aided in the structural ordering (and catalytic activity) to a greater degree than when using Ar alone, which is consistent with previous observations for Pt-based bimetallic alloys[1-2]. The annealing time was based on catalytic activity and electrochemical surface area screening; where shorter (0.5 h) and longer (2 h) were slightly inferior to 1 h annealed samples.

The FePt(1:1)/C sample was also acid-treated in order to mimic a dealloying phenomenon that occurs under repeated catalytic cycles[3]. An entire batch of the sample was treated in 0.5 M HNO_3 by first dispersing it by 30 min sonication. Then the dispersion was heated to 70 ^oC overnight under stirring after which the sample was washed with copious amounts of $(H_2O)_{DI}$ and ethanol and dried at 60 ^oC hotplate. XRD and ORR performance was then recorded for this sample according to the procedures described below.

Nitrogen doped reduced graphene oxide (NrGO) was also synthesized to investigate the MW synthesis influence of catalyst support. NrGO was prepared by thermal exfoliation of Tours graphene oxide ("Improved" Hummers method)[4] prepared with natural flake graphite (Alfa Aesar -100 mesh, briquetting grade), in presence of ammonia[5]. Specifically, freeze-dried GO powder was

inserted into a tube furnace and saturated in ammonia gas (80 ml min^{-1}) combined with an Ar carrier gas (100 ml min^{-1}). The temperature was then ramped up to 750 ^{o}C over the course of 20 min and maintained for 1 h. The resulting NrGO support was then directly used for supporting FePt NPs by following the above procedure but with a 1 min MW treatment in step (i) due to excessive heat build-up. Moreover, the metal loading was set to 40 wt. % to compensate for the relatively high surface area to volume ratio of NrGO, enabling electrochemical experiments with the same Pt-loading.

Calculation of order parameter

The order parameter (S*) is a direct measure of the degree of ordering in FePt alloys (relative abundance of the $L1_0$-fct phase), as reported by Sakuma H. et al.[6], and was used to trace the disorder-to-order transformation in the MW annealing experiment. S^* is provided according to

$$S^{*2} = \frac{I_s}{I_f}, \quad \text{(S1)}$$

where I_s is the intensity of the superstructure reflection and I_f is the intensity of the fundamental reflection. $S^* = 1$ for 100% ordered structures which then fix the intensity ratio $(I_s/I_f)_{std}$ and allows to evaluate the order parameter of a partially-ordered material by

$$S_{hkl}^{*2} = \frac{\left(I_{hkl}/I_{111}\right)_{exp}}{\left(I_{hkl}/I_{111}\right)_{std}}, \quad \text{(S2)}$$

where the subscripts "exp" and "std" relates to the experimental sample and the standard (reference) material, while "*hkl"* refers to the selected superstructure peak. In our case, we used the (110) and (111) pair as superstructure and fundamental peaks. We did not use the common (001)/(111) pair owing to the broad (001) peaks that was not clearly separated in our XRD patterns. The fully ordered intensity ratio ($(I_{hkl}/I_{111})_{std}$) was calculated from a simulated XRD pattern using an fct crystal structure with lattice parameters a = 3.861 Å and c = 3.788 Å, resulting in an intensity ratio of 0.30 and 0.25 for the $(I_{001}/I_{111})_{std}$ and $(I_{110}/I_{111})_{std}$ peaks, respectively, in agreement with other reports. The results are presented in table S1.

Computational details

Spin-polarized *ab initio* theoretical computations were performed on cuboctahedral nanoparticles containing 147 atoms. These cuboctahedrons have a midsphere radius of 8.55 Å (~1.7 nm diameter) considering an edge length, a, of 9.873 Å. Three different nanoparticles were used to evaluate the mass activity, these were a Pt_{147}, a fct FePt(1:0.8)@Pt, and a fcc FePt(1:0.9)@Pt cuboctahedrons. An atom-thin Pt shell was kept for both FePt@Pt particles. The fct FePt@Pt cuboctahedron was prepared by replacing Pt atoms by Fe in alternated layer along the (100) direction similar to the fct bulk phase. The fcc FePt@Pt cuboctahedron was prepared by randomly replacing Pt atoms by Fe in the core. To account for the effect on random Fe distribution, five different systems were

prepared, the selected model exhibited the lowest formation energy. Exchange–correlation effects are approximated by the revised Perdew, Burke and Ernzerhof[7] functional. The wave functions for the valence electrons are represented by a linear combination of pseudo-atomic numerical orbitals using a double-ζ plus one polarized orbital basis set. The sampling for the Brillouin zone is done only at the gamma point. A Methfessel–Paxton smearing of 0.1 eV and Pulay mixing are employed to aid convergence on the self-consistent electron density. The real-space grid used for charge and potential integration is equivalent to a plane wave cut-off energy of 250 Ry. The position of the ionic cores are allowed to relax until the maximum force component is <0.04 eV $Å^{-1}$. All computations were performed using the SIESTA code[8].

The catalytic activity was evaluated by first calculating the adsorption free energy ($\Delta G_{OH,X}$) of the OH intermediate using

$$\Delta G_{OH,X} = \Delta E_{OH,X} + \Delta E_{ZPE} - T\Delta S \quad \text{(S3)}$$

where $\Delta E_{OH,X}$ is the OH-adsorption energy, ΔE_{ZPE} is the difference in zero point energy, T is the temperature, and ΔS is the change in entropy. The sub index "X" indicates the type of adsorbent. The adsorption energy of the OH intermediate ($\Delta E_{OH,X}$) was calculated using H_2O and H_2 in the gas phase as reference states using,

$$\Delta E_{OH,X} = E_{OH+NP} + \frac{1}{2}E_{H2} - E_{H2O} - E_{NP} \quad \text{(S4)}$$

where E_{NP}, E_{OH+NP}, E_{H2}, and E_{H2O}, are the energies of the isolated particle, particle with the adsorbed OH intermediate, hydrogen, and water molecule. Considering that the contributions from the zero point energy and entropy are similar on all systems (Pt_{147}, fct and fcc FePt), the adsorption free energy difference relative to Pt(111) was reduced to

$$\Delta G_{OH,X} - \Delta G_{OH,Pt111} = \Delta E_{OH,X} - \Delta E_{OH,Pt111} \quad \text{(S5)}$$

Similar approach has been previously used[9]. The catalytic activity relative to Pt(111), $\ln(j/j_{Pt111})$, was then evaluated by using the difference in OH adsorption free energy ($\Delta G_{OH,X}$ - $\Delta G_{OH,Pt111}$) at diverse active sites along the cuboctahedral particles using the following expressions:

$$ln\left(j/j_{Pt111}\right) = 16.39(\Delta G_{OH,X} - \Delta G_{OH,Pt111}) + 0.15 \quad \text{(S6)}$$

$$ln\left(j/j_{Pt111}\right) = 4.98 - 25.89(\Delta G_{OH,X} - \Delta G_{OH,Pt111}) \quad \text{(S7)}$$

These expressions were based on the work by Gagliardi and co-workers[10], but these were adapted to correlate the catalytic activity with the free energy of adsorption instead of the generalized coordination numbers ($\overline{CN}$) as they do in their work. Similar expressions have been reported by Nørskov and co-workers[9], however the one reported by Gagliardi is a direct fitting from experimental ORR activity at 0.9 V vs RHE relative to Pt(111). The first expression represent the left side of the Volcano plot (strong OH adsorption), while the second expression represents the

right side (weak OH adsorption). Both expressions were evaluated, and the smallest activity, MIN(ln(j/j_{Pt111})), was used to construct the Volcano plot. This same value was also used to evaluate the theoretical mass activity (MA) in A/mg_{Pt} using the following equation:

$$MA(A/mg_{Pt}) = \frac{\sum_{i=1}^{N} j}{(\rho_{Pt111} * M_{Pt} * N_{Pt} * 10^6)} \quad \text{(S8)}$$

where the j was evaluated using the experimental value of j_{Pt111} of 2 mA/cm^2_{Pt} [11], as indicated below:

$$j = j_{Pt111} e^{MIN(ln(j/j_{Pt111}))} \quad \text{(S9)}$$

The sum runs over all active sites with a difference in OH adsorption free energy ($\Delta G_{OH,X}$ - $\Delta G_{OH,Pt111}$) in the range of 0.00 to 0.15 to minimize the error[10]. ρ_{Pt111} is the Pt(111) surface density of 1.503×10^{15} atoms/cm^2, M_{Pt} is the Pt atomic mass of 3.2395×10^{-22} g, and N_{Pt} is the total number of Pt atoms in the nanoparticles (147 for pure Pt, 116 for the fct particle, and 121 for the fcc system). The factor of 10^6 is used to convert mA/g_{Pt} to A/mg_{Pt}. The results are listed in the table S6.

Supplementary results

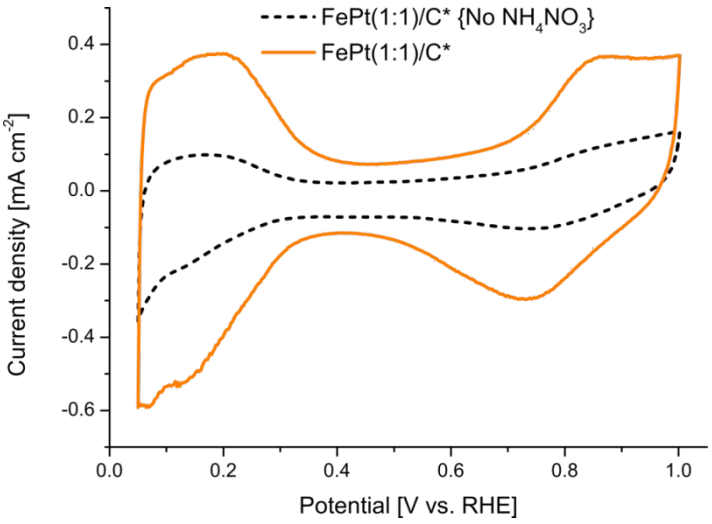

Fig. S1. *ECSA curves recorded in Ar saturated $HClO_4$ (H_{UPD}) comparing FePt(1:1)/C* and a sample with omitted oxidant (NH_4NO_3) (dashed lines). Note: the latter sample was prepared with a reaction time of 1 min due to excessive heat build-up. Overall, samples with no ammonium nitrate showed significantly lower ECSA, in line with our previous observations[12]. XRD peaks of samples without NH_4NO_3 remained broad, supporting that NP sizes are determined mainly by iron content, implying that measured ECSA does not likely stem from a NH_4NO_3-induced "carbon-activation/functionalization" effect and can safely be attributed to oxidative removal of carbonaceous ligand residue.*

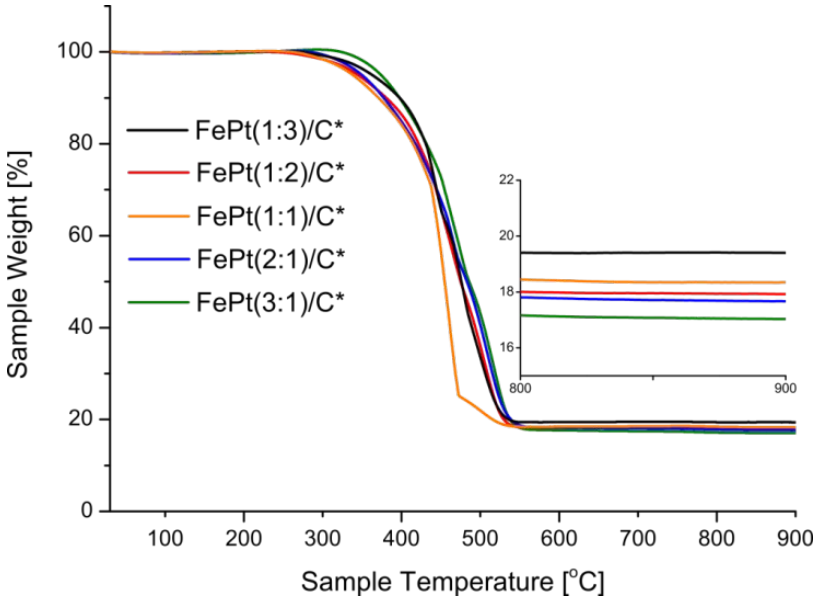

Fig. S2. *TGA measurements in air of respective FePt(X:Y)/C* samples for the purpose of estimating metal loading. No difference between FePt(1:1)/C* and FePt(1:1)/C was observed and the target loadings (20 wt.%) were approximately met for all samples, strengthening the assumption of nearly full preservation of the initial precursor composition. The slightly lower loading, in contrast to our previous observations[12], can likely be attributed to the heavier organic ligand in $Fe(acac)_3$ as supported by the declining trend in metal loading with increased Fe.*

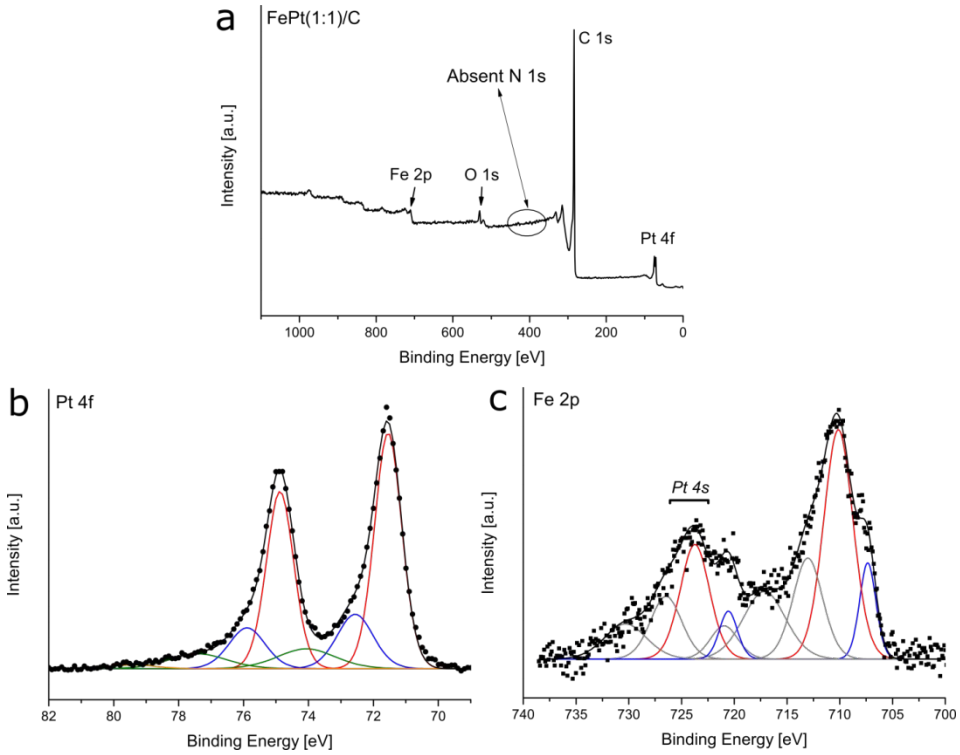

Fig. S3. *XPS spectra of FePt(1:1)/C including survey spectra (a) and high resolution spectra of Pt 4f (b) and Fe 2p (c) core-level regions. No traces of NH_4NO_3 was found and the estimated surface metal atomic ratio (Fe:Pt) was 1.16:1.00. The Pt 4f $_{7/2}$ region (b) shows three predominant species: metallic Pt (~71.5 eV), Pt-C (~72.5 eV) and Pt-O (~74.0 eV). The Fe 2p 3/2 region show mainly two species (c) assigned to metallic Fe (~707.4 eV) and Fe=O (710.1 eV) as well as overlapping satellite peaks (Gray) and potential Pt 4s overlap (highlighted region).*

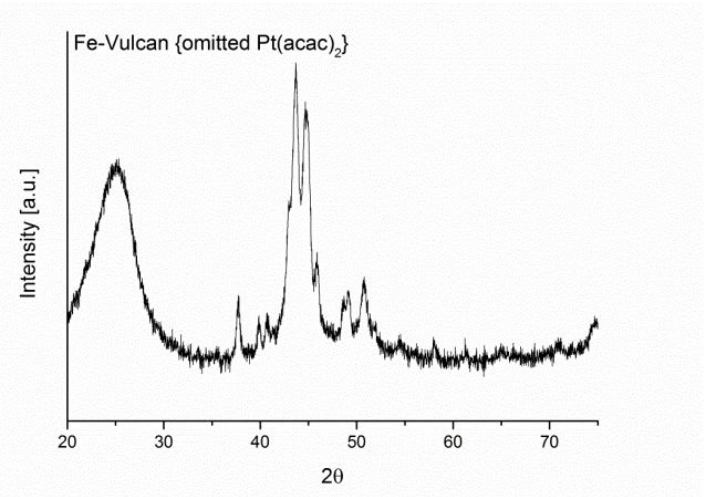

Fig. S4. *Background XRD pattern of sample produced with 20 wt.% Fe (without Pt-precursor).*

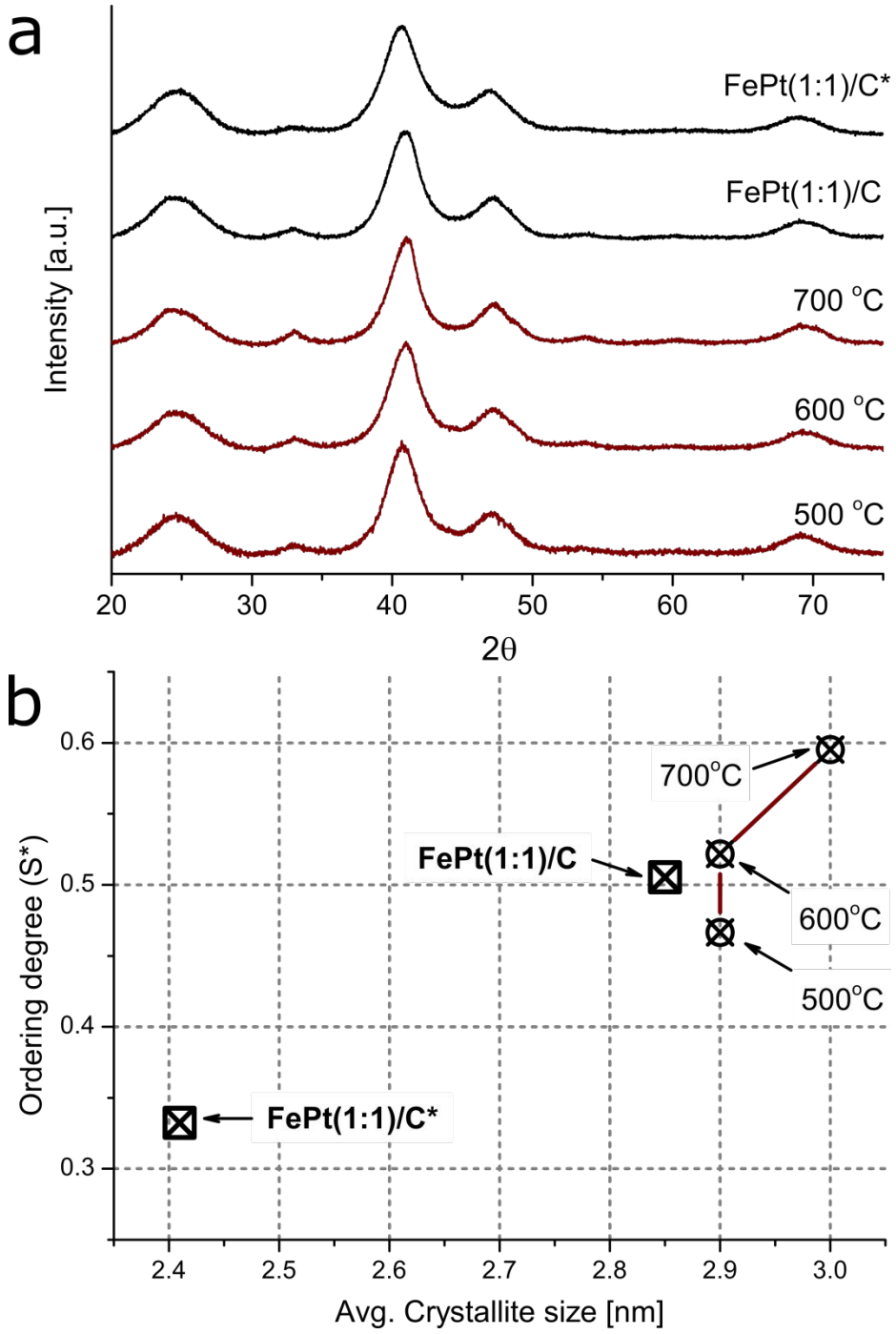

Fig. S5. *XRD patterns comparing FePt(1:1)/C and FePt(1:1)/C* with the FePt(1:1)/C* sample annealed for 1 h in 5 % H_2 in Ar by conventional heating in a tube furnace (a) at three different temperatures (500, 600 and 700 °C). Corresponding degree of ordering represented by the S* parameter, extracted from the (110)/(111) intensity ratio by equations S1-S2, versus crystallite size is shown in (b) where all samples stayed below 3 nm, suggesting a good resilience toward NP migration and coalescence (see table S2 for literature comparison).*

Table S1. *Order parameter S of FePt (1:1) samples where other studies are included for comparison. We can here conclude that the MW annealing improves fct ordering from 33% to 51%. Note: in the other listed references, the average sizes of the crystallites are larger.*

FePt(1:1) (Ref.)	**Annealing temperature (°C)**	**$I(110)/I(111)_{exp}$**	**S***
This work	FePt(1:1)/C* (**before** MW annealing)	0.0276	0.33 (S^*_{110})
	FePt(1:1)/C (**after** MW annealing, 400W)	0.0635	0.51 (S^*_{110})
	FePt(1:1)/C (**after** MW annealing, 640W)	0.099	0.63 (S^*_{110})
	500	0.0540	0.47 (S^*_{110})
	600	0.0677	0.52 (S^*_{110})
	700	0.0876	0.59 (S^*_{110})
[13]	400	-	0 (S^*_{001})
	500	-	0.5397 (S^*_{001})
	600	-	0.6708 (S^*_{001})
	700	-	0.9626 (S^*_{001})
	750	-	0.9998 (S^*_{001})
[14]	600	-	0.66 (S^*_{001})

Table S2. *Overview of NP size increments as a result of annealing found in literature. The relatively low NP size enlargement suggests a firm attachment of NPs to the support as a result of the microwave treatment, supported by Fig. S5 and our previous result for Pt_3Co/C where similar conditions were used (~3.2 to 3.4 nm)[12]. This table is limited to carbon supported (substrate) FePt nanoparticles and all presented samples have an approximate atomic composition of 1:1. Note: ref.[15] also demonstrated a Pt_3Fe/C catalyst with NP growth to only ~6.8 nm attributed to a protective carbonaceous coating.*

Synthesis method	Temperature (°C)	Annealing time (min)	Atmosphere	Initial NP size (nm)	Final NP size (nm)	Reference
Microwave	700	60	Ar + 5 % H_2	2.4	3.0	[This study]
Solvothermal	500	20	H_2	~6	~8	[16]
Solvothermal	500	20	N_2	~6	~14	[16]
Ion beam sputtering	650	60	Vacuum	3	7	[17]
Polyol + annealing	600	180	Ar + 8 % H_2	2.1	4.2	[18]
Polyol + annealing	800	180	Ar + 8 % H_2	2.1	6.1	[18]
Solvothermal	700	?	Ar + 4 % H_2	~5.6	~10.8	[15]
Polyol + annealing	700	120	Ar + 10 % H_2	~4.1	~5.8	[1]

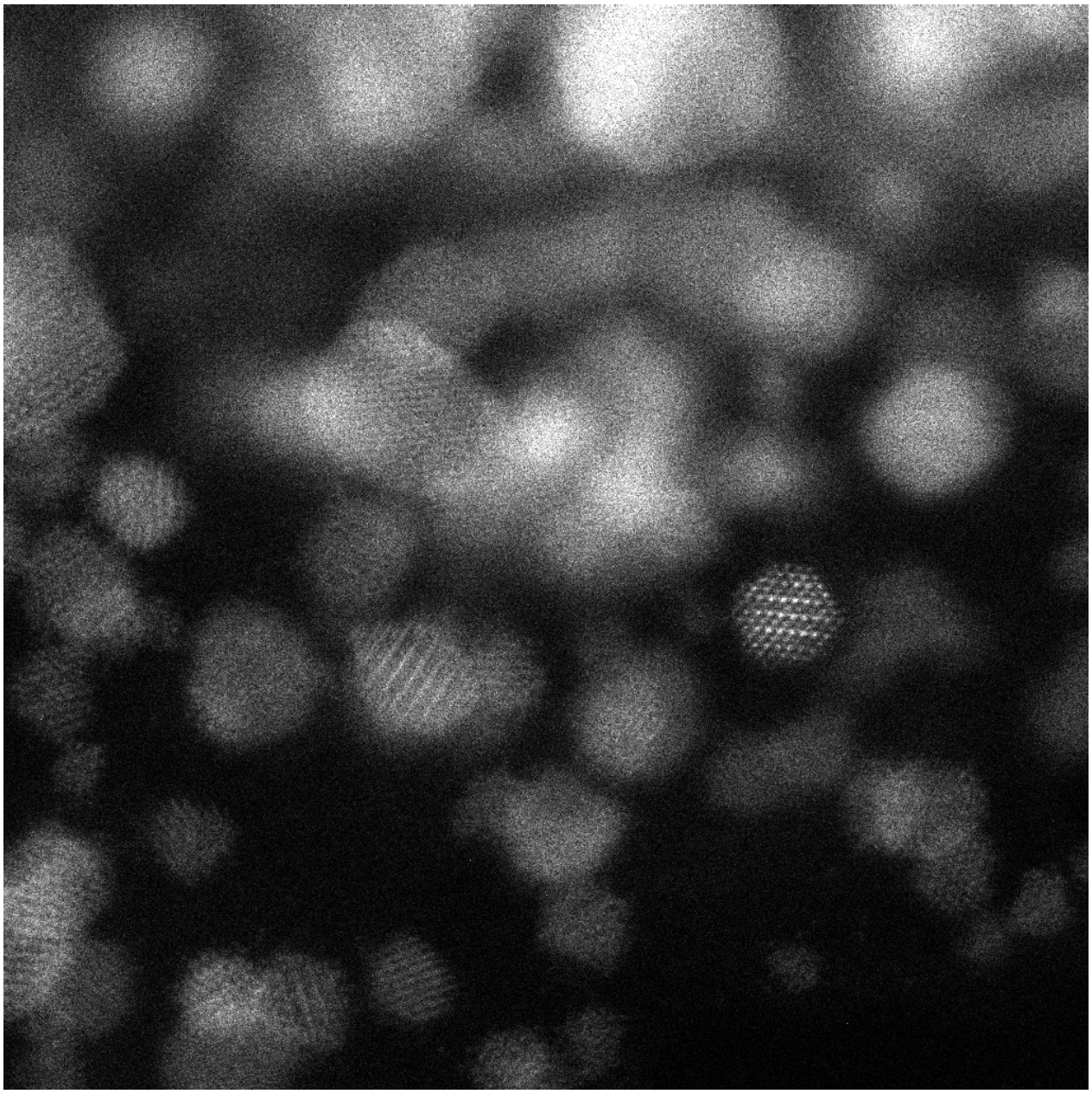

Fig. S6. *Low cameralength high resolution HAADF-STEM image of the same area as shown in Fig. 2. The reduced camera length reduces the signal strength, but promotes mass contrast. As can be seen, the apparent laminated appearance of some particles remains, indicating a separation between heavy elements (Pt) and lighter elements (Fe).*

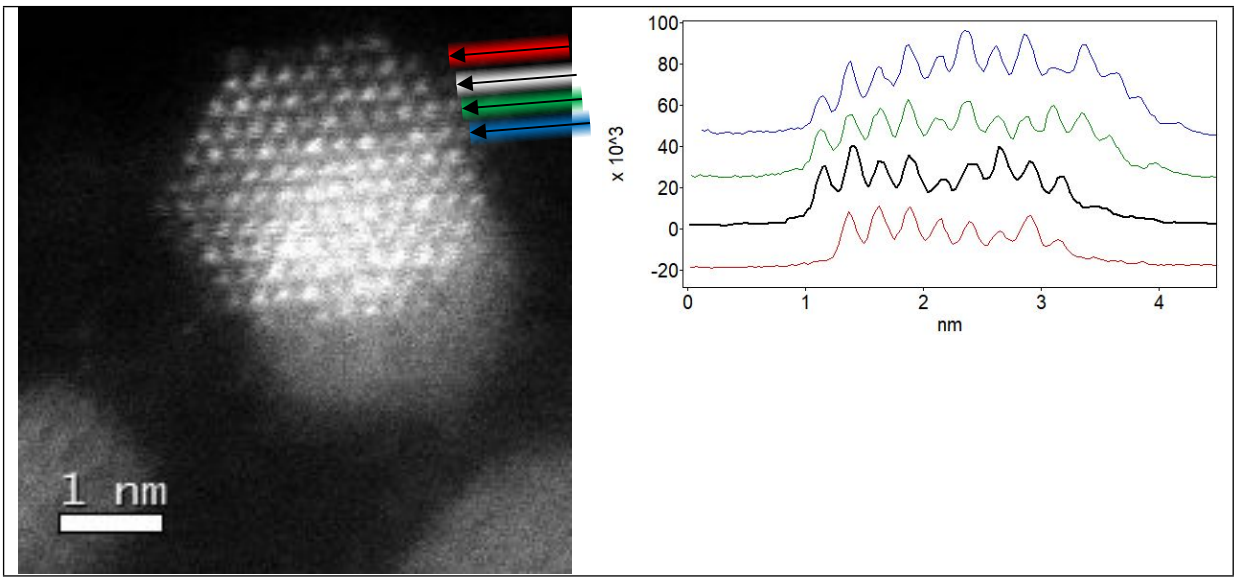

Fig. S7. *HAADF-STEM of atomic columns within an fcc particle found in the FePt(1:1)/C sample with corresponding intensity profile. The random intensities suggest a solid solution, thus supporting successful Fe incorporation. This observation, in combination with the observed fct particles (Fig. S6), further validates likely surface facets modelled in the ORR dft calculations.*

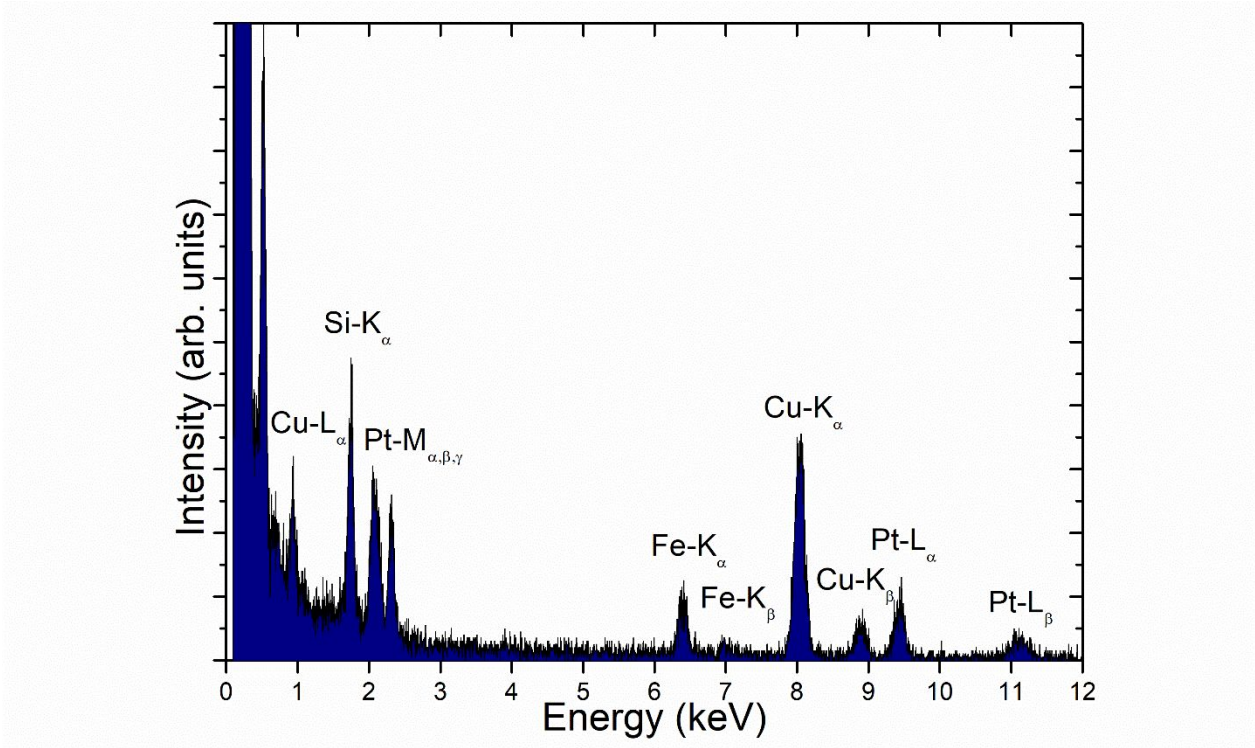

Fig. S8. *EDX spectrum obtained from an average of ~20 particles, ranging from 2-4 nm in diameter quantification of the spectrum using F-K and Pt-L lines yields a near 1:1 ratio, see table S3-S4. Si and Cu are system artefacts and the excessive C-K peak (beyond the scale) originates from the C support. Quantification was performed using the TIA software.*

Table S3. *EDX data obtained from a cluster of ~2-4 nm NPs.*

Element	Weight %	Atomic %	Uncert. %
Fe(K)	20.77	47.80	1.19
Pt(L)	79.22	52.19	2.95

Table S4. *EDX data obtained from a cluster of ~5-7 nm NPs.*

Element	Weight %	Atomic %	Uncert. %
Fe(K)	13.48	35.26	0.29
Pt(L)	86.51	64.73	1.02

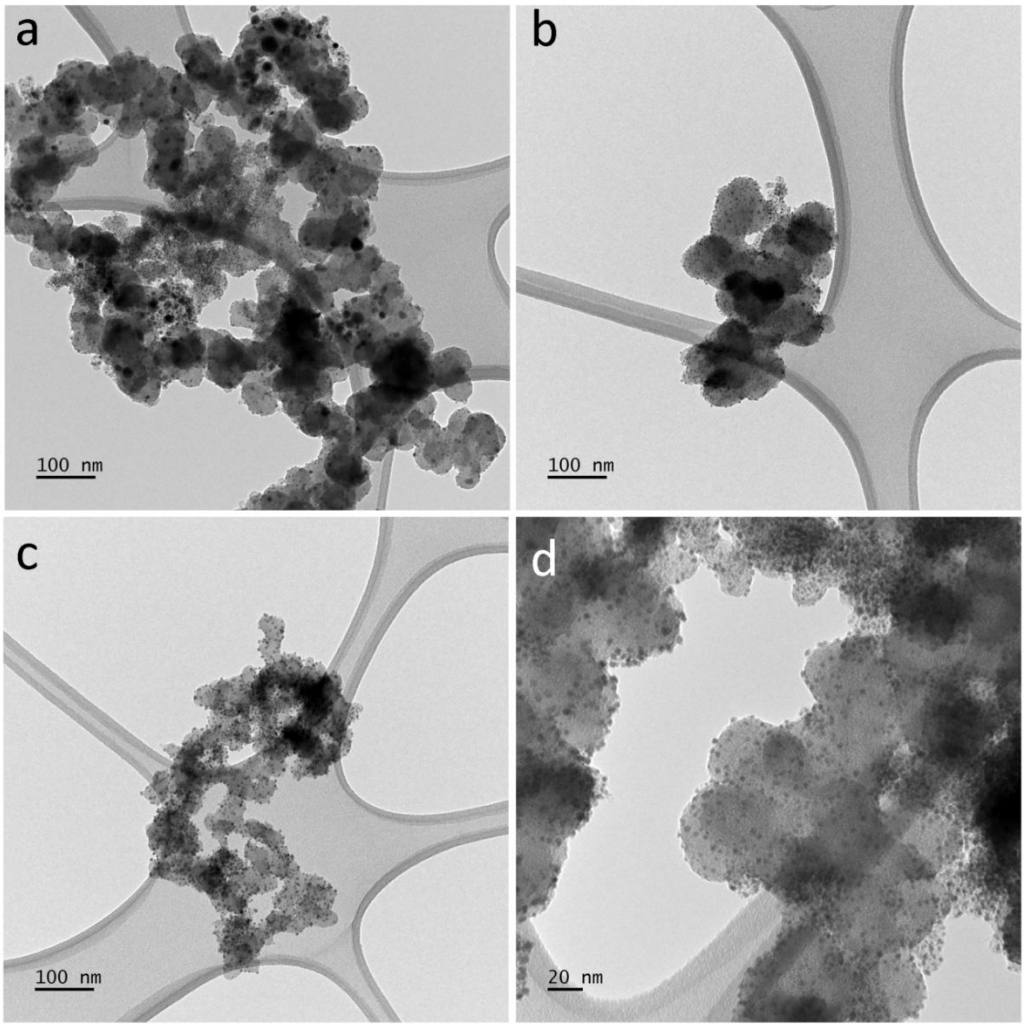

Fig. S9. *Low-resolution TEM images for FePt(1:1)/C of four representative regions (a-d) showcasing diverse decoration qualities and NP size distribution. Majority regions constitute small and evenly distributed NPs in line with the broad FWHMs in the XRD pattern and the 1-4 nm range in Fig. S10.*

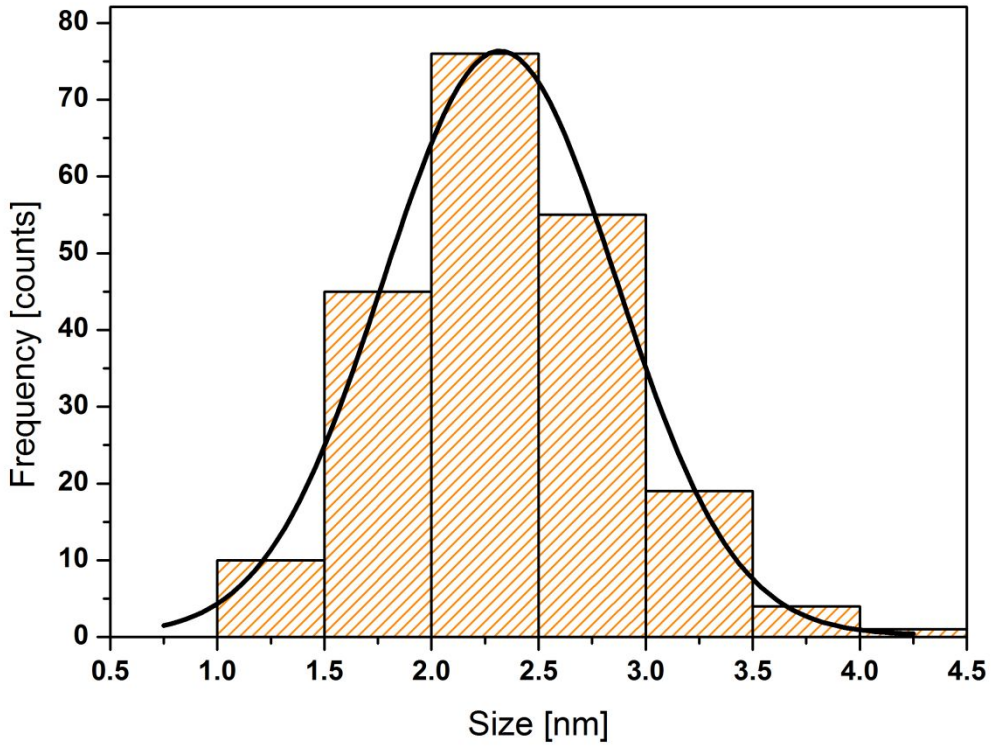

Fig. S10. *Particle size distribution of the FePt(1:1)/C sample with an average particle size of 2.3 +/- 0.6 nm, as calculated from multiple TEM images in the majority regions with smaller NPs. The small discrepancy to XRD (2.9 nm) can be explained by the formation of larger NP aggregates during annealing that is only scarcely seen on the TEM grid; causing peak narrowing.*

Table S5. *Kinetic currents (j_k) measured at 0.9 V vs. RHE in O_2 saturated $HClO_4$ at a rotational rate of 1600 rpm. Background correction and iR-compensation was performed post measurement.*

FePt(3:1)/C*	FePt(2:1)/C*	FePt(1:1)/C*	FePt(1:2)/C*	FePt(1:3)/C*	FePt(1:1)/C	Pt/C
0.264 *mA*	0.462 *mA*	0.983 *mA*	0.973 *mA*	0.770 *mA*	1.596 *mA*	0.850 *mA*

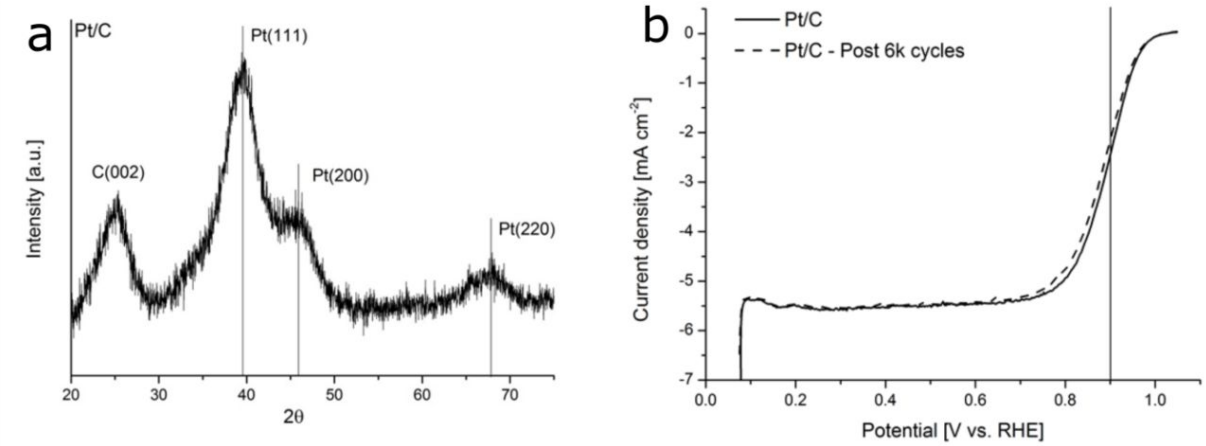

Fig. S11. *XRD pattern of Pt/C (a) (commercial sample) where NP sizes can be estimated to ~1.8 nm. LSV characteristics of Pt/C with the LSV profile post 6000 cycles between 0.6 and 1.0 V vs. RHE in O_2 saturated $HClO_4$ (b). The accelerated degradation test resulted in an 18 % loss of j_k, and as a consequence, the same loss in MA.*

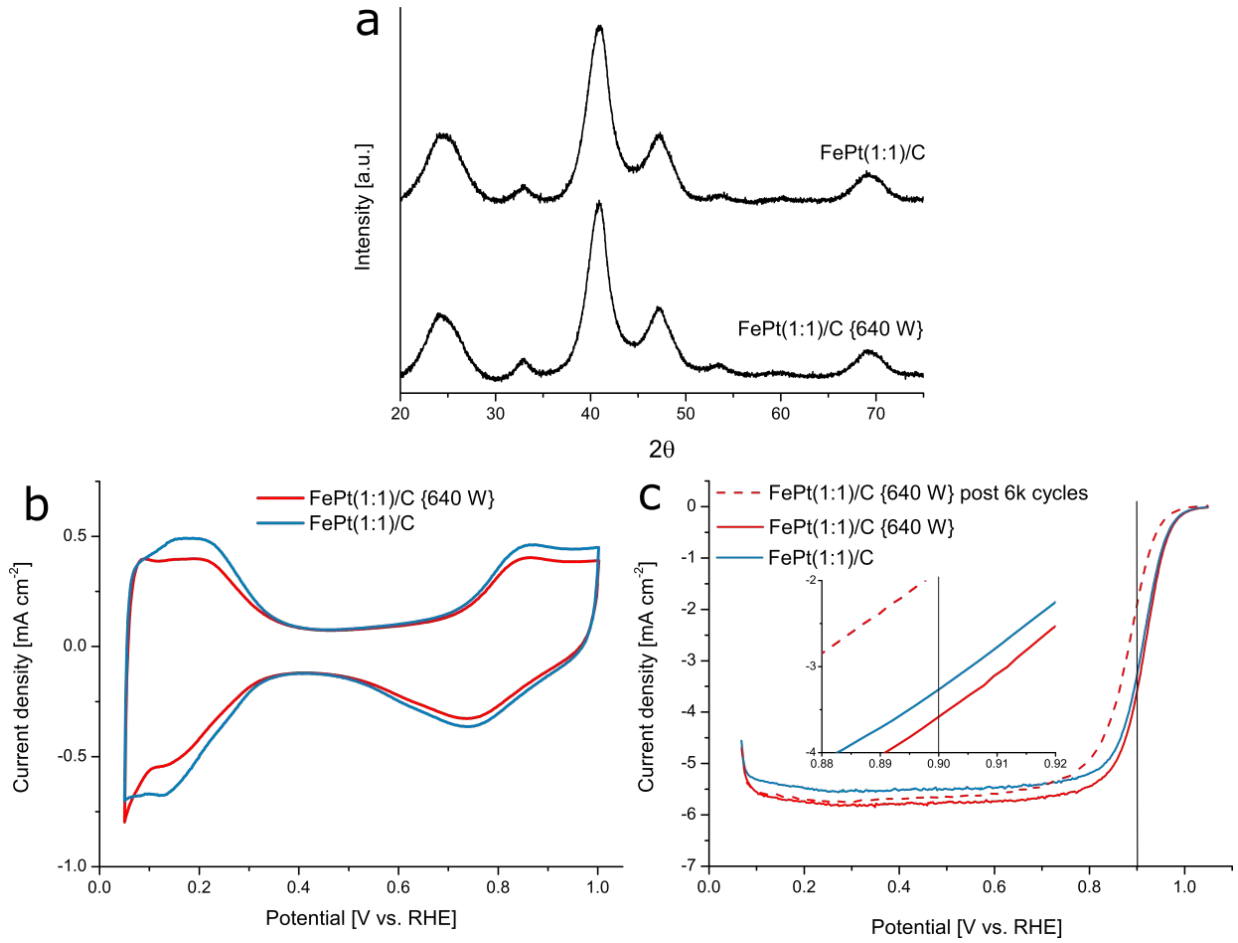

Fig. S12. *XRD (a) and ORR performance survey (b-c) of FePt(1:1)/C prepared with 80 % power (640 W) in the secondary microwave annealing step compared to the 50 % power (400 W) (FePt(1:1)/C) used in this study. The intensity shows an* $(I_{110}/I_{111})_{exp}$ of 0.099 corresponding to 63% ordering. *Although showing initially better activity than FePt(1:1)/C with* MA ≈ 650 A/g_{Pt}, *the sample lost a significant activity after 6000 cycles in* O_2 *saturated electrolyte between 0.6 and 1.0 V vs. RHE. The average NP size calculated by the Scherrer formula was ~3.0 nm and the ordering degree was similar to the sample annealed at 700 °C in Fig. S5. The electron transfer number was measured to n=3.8.*

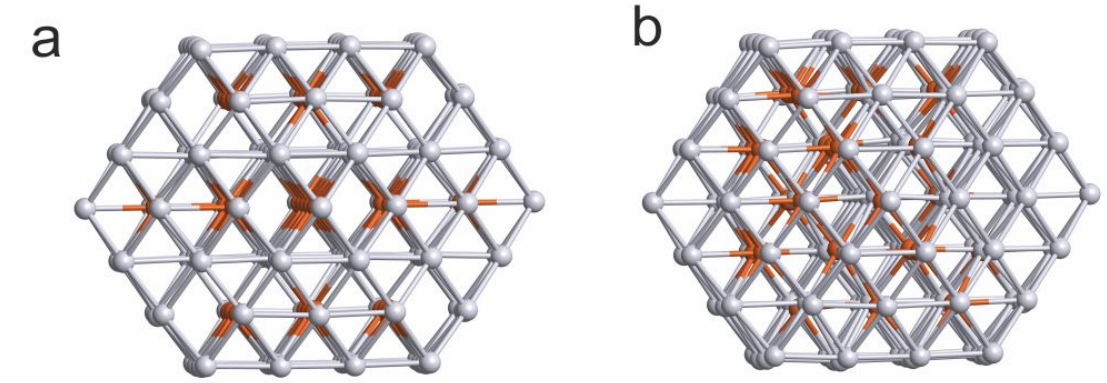

Fig. S13. *FePt cubochatedrons used to evaluate the theoretical mass activity. (a) fct FePt@Pt cuboctahedron. (b) fcc FePt@Pt cuboctahedron. The catalytic active site was the Pt atom located at the center of the (111) surfaces. In this case there are only eight of such atoms. All eight atoms in the fct particles are equivalent, while in the fcc all eight sites are unique. All sites are used to estimate the mass activity.*

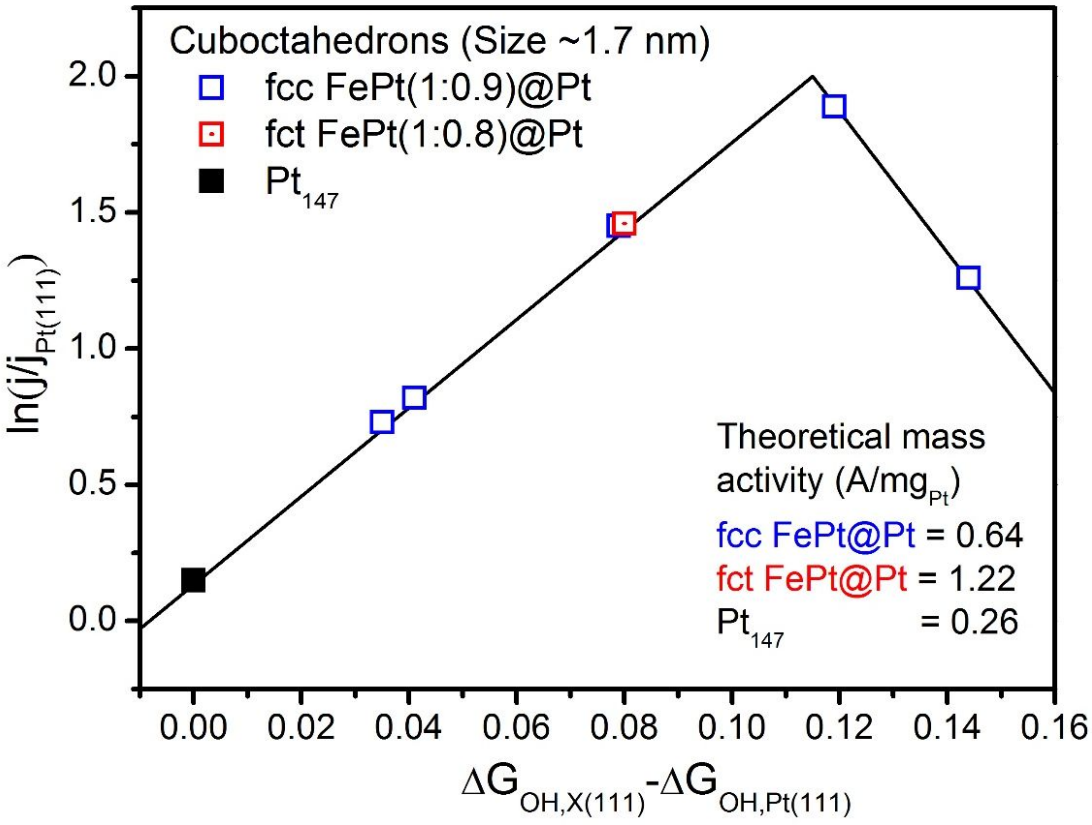

Fig. S14. *Activity volcano plot for ORR relative to pure Pt(111). For Pt_{147} and fct FePt@Pt all active are equivalent, thus a single point is seen in the plot. For fcc FePt@Pt, five sites lies within the selected OH-adsorption range.*

Table S6. *Theoretical mass activities. Note that Pt_{147} and fct FePt@Pt are highly symmetric so there is only one non-equivalent site located at the (111) surface, however there are 8 sites, so the sum term in the MA calculation ($\sum_{i=1}^{N} j$) goes up to 8. In the case of the fcc FePt@Pt, all 8 sites were tested, but only 5 exhibit a difference in adsorption energy ($\Delta G_{OH,X}$ - $\Delta G_{OH,Pt111}$) in the range of 0.00 to 0.15. The rest exhibit too weak adsorption energies to significantly contribute to the MA.*

System	$\Delta G_{OH,X}$- $\Delta G_{OH,Pt111}$ (eV)	MIN(ln(j/j_{Pt111}))	$\sum_{i=1}^{N} j$ (mA/cm²)	Theoretical MA (A/mg_{Pt})	Experimental MA (A/mg_{Pt})
Pt_{147}	0.00	0.15 (8 sites)	18.59	0.26	0.212
fct FePt@Pt	0.08	1.46 (8 sites)	68.90	1.22	0.57
fcc FePt@Pt-site-1	0.12	1.89	37.44	0.64	0.351
fcc FePt@Pt-site-2	0.40	0.73			
fcc FePt@Pt-site-3	0.14	1.26			
fcc FePt@Pt-site-4	0.08	1.45			
fcc FePt@Pt-site-5	0.04	0.82			

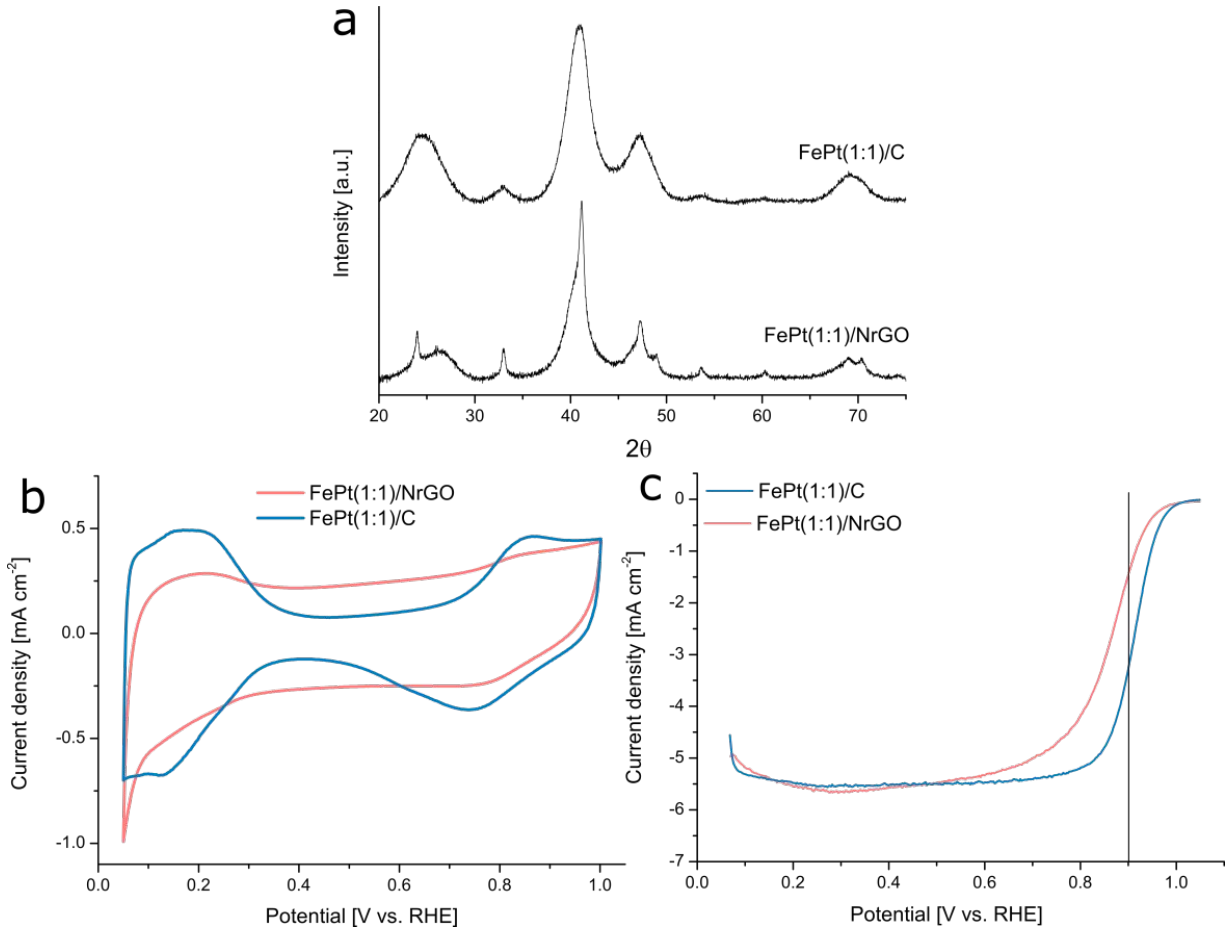

Fig. S15. *XRD (a) and ORR performance survey (b-c) of FePt(1:1)/NrGO compared with FePt(1:1)/C used in this study (GC electrodes are here prepared with the same Pt loading). The overall ECSA and ORR performance of FePt(1:1)/NrGO is poor, likely attributed to the emerging sharp peaks in the diffractogram indicating presence of large NP sizes. A two peak model of the (220)/(202) region yields NP sizes of 3.0 nm and 17 nm by using the FWHM from respective peaks. The S* parameter, considering the absolute intensities, was 0.81. The Pt(111) reflection in (a) does however contain a broad shoulder in addition to a sharper reflection, suggesting that high degree of ordering was achieved on larger particles considering that all fct reflections have such sharp profile. The pronounced diversity in NP sizes is seen also in Fig. S16.*

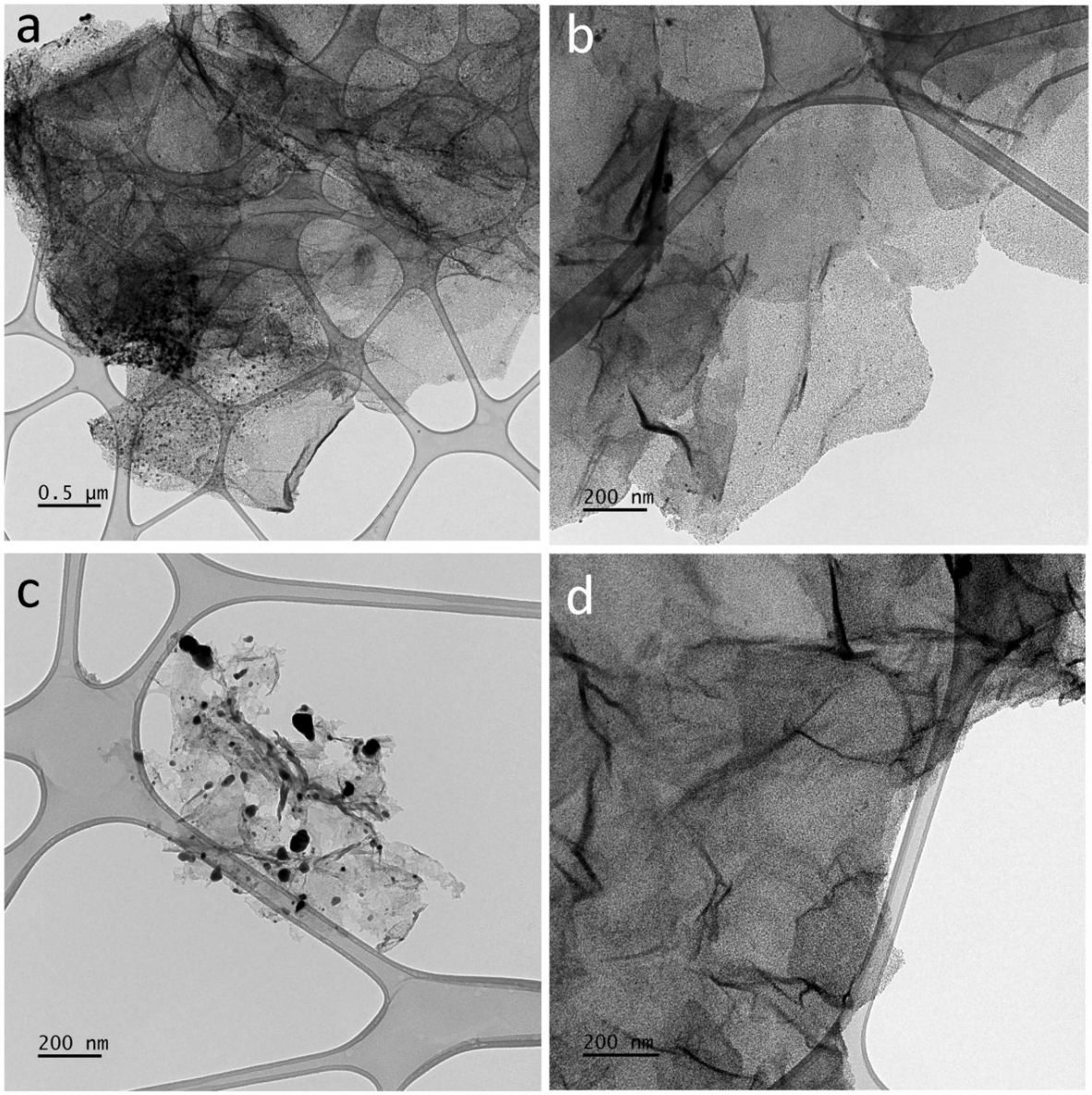

Fig. S16. *Survey of decoration by* ***l****ow-resolution TEMs showing representative regions of the FePt(1:1)/NrGO sample (a-d). A significant diversiy in NP sizes were detected ranging from several tens on nanometres to finely distributed few-nanometre NPs on some flakes with remarkable decoration. Typically, smaller flakes and regions with severe "folding" showed larger NPs. These results combined with the observations in Fig. S15 suggest that the MW method is sensitive to the support, hence using a well-defined carbon support is advisable.*

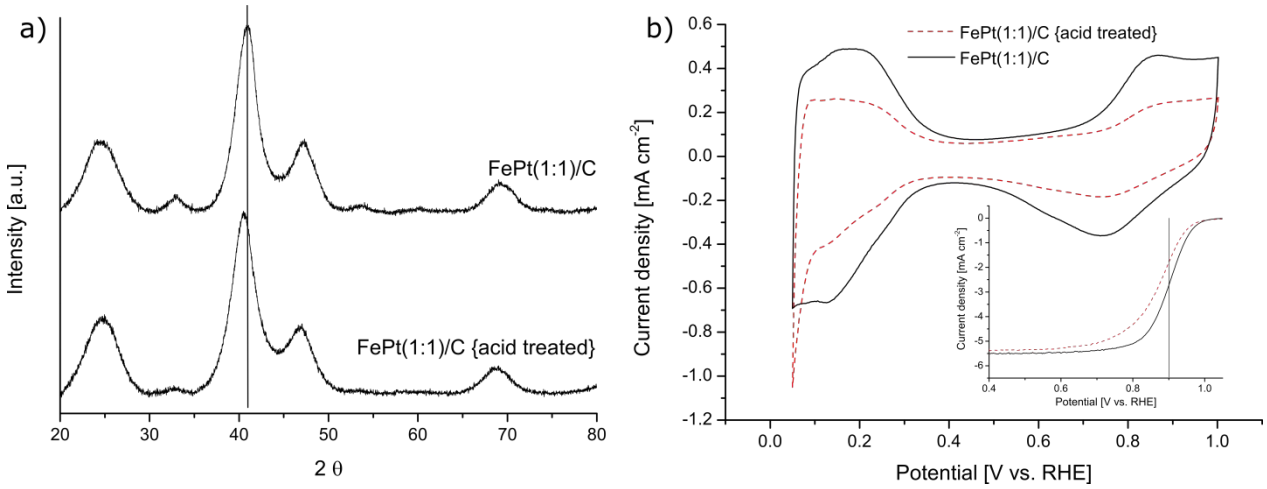

Fig. S17. *XRD (a) and ECSA (b) evaluation of acid treated (HNO_3) FePt(1:1)/C where the inset shows the LSV profiles in O_2 saturated $HClO_4$. The order parameter (S*) dropped from 0.51 to 0.36. An average NP size drop from 2.9 to 2.5 nm along with a slight downshift in all fcc reflections after acid treatment support that dealloying and leaching of Fe occurred. ORR evaluation showed a decrease of 58 % of initial mass activity and an ECSA drop measured by H_{UPD} from ~52 to ~42 m^2/g_{Pt}. Note: the use of controlled post-treatment dealloying experiments to potentially favor the catalytic performance should not be discouraged.*

References

(1) Moradi, R.; Sebt, S. A.; Arabi, H. Size Controlling of L10-Fept Nanoparticles During High Temperature Annealing on the Surface of Carbon Nanotubes. *J. Inorg. Organomet. Polym. Mater.* **2016,** *26*, 344-352.

(2) Jung, W. S.; Popov, B. N. Effect of Pretreatment on Durability of Fct-Structured Pt-Based Alloy Catalyst for the Oxygen Reduction Reaction under Operating Conditions in Polymer Electrolyte Membrane Fuel Cells. *ACS Sustainable Chem. Eng.* **2017,** *5*, 9809-9817.

(3) Wang, J. M.; Wang, Z. L.; Li, S.; Wang, R. M.; Song, Y. J. Surface and Interface Engineering of Fept/C Nanocatalysts for Electro-Catalytic Methanol Oxidation: Enhanced Activity and Durability. *Nanoscale* **2017,** *9*, 4066-4075.

(4) Marcano, D. C.; Kosynkin, D. V.; Berlin, J. M.; Sinitskii, A.; Sun, Z.; Slesarev, A.; Alemany, L. B.; Lu, W.; Tour, J. M. Improved Synthesis of Graphene Oxide. *ACS Nano* **2010,** *4*, 4806-4814.

(5) Poh, H. L.; Šimek, P.; Sofer, Z.; Tomandl, I.; Pumera, M. Boron and Nitrogen Doping of Graphene Via Thermal Exfoliation of Graphite Oxide in a Bf3 or Nh3 Atmosphere: Contrasting Properties. *J. Mater. Chem. A* **2013,** *1*, 13146-13153.

(6) Sakuma, H.; Taniyama, T.; Ishii, K.; Kitamoto, Y.; Yamazaki, Y. Analysis of Atomic Arrangement in Magnetic Fe–Pt Nanoparticles. *J. Magn. Magn. Mater.* **2006,** *300*, 284-292.

(7) Hammer, B.; Hansen, L. B.; Nørskov, J. K. Improved Adsorption Energetics within Density-Functional Theory Using Revised Perdew-Burke-Ernzerhof Functionals. *Physical Review B* **1999,** *59*, 7413-7421.

(8) Soler, J. M.; Artacho, E.; Gale, J. D.; García, A.; Junquera, J.; Ordejón, P.; Sánchez-Portal, D. The Siesta Method Forab Initioorder-Nmaterials Simulation. *J. Phys.: Condens. Matter* **2002,** *14*, 2745-2779.

(9) Viswanathan, V.; Hansen, H. A.; Rossmeisl, J.; Nørskov, J. K. Universality in Oxygen Reduction Electrocatalysis on Metal Surfaces. *ACS Catal.* **2012,** *2*, 1654-1660.

(10) Rück, M.; Bandarenka, A.; Calle-Vallejo, F.; Gagliardi, A. Oxygen Reduction Reaction: Rapid Prediction of Mass Activity of Nanostructured Platinum Electrocatalysts. *The Journal of Physical Chemistry Letters* **2018,** *9*, 4463-4468.

(11) Calle-Vallejo, F.; Tymoczko, J.; Colic, V.; Vu, Q. H.; Pohl, M. D.; Morgenstern, K.; Loffreda, D.; Sautet, P.; Schuhmann, W.; Bandarenka, A. S. Finding Optimal Surface Sites on Heterogeneous Catalysts by Counting Nearest Neighbors. *Science* **2015,** *350*, 185.

(12) Sandström, R.; Ekspong, J.; Gracia-Espino, E.; Wågberg, T. Oxidatively Induced Exposure of Active Surface Area During Microwave Assisted Formation of Pt3co Nanoparticles for Oxygen Reduction Reaction. *RSC Advances* **2019,** *9*, 17979-17987.

(13) Medwal, R.; Sehdev, N.; Annapoorni, S. Order–Disorder Investigation of Hard Magnetic Nanostructured Fept Alloy. *J. Phys. D: Appl. Phys.* **2012,** *45*, 055001.

(14) Kalyan Kamal, S. S.; Sahoo, P. K.; Durai, L.; Ghosal, P.; Ram, S.; Raja, M. Study of Fe-Rich Fept Nanoparticles Synthesized by a Single Step Reverse Micelle Route. *J. Alloys Compd.* **2010,** *501*, 297-300.

(15) Jung, C.; Lee, C.; Bang, K.; Lim, J.; Lee, H.; Ryu, H. J.; Cho, E.; Lee, H. M. Synthesis of Chemically Ordered Pt3fe/C Intermetallic Electrocatalysts for Oxygen Reduction Reaction with Enhanced Activity and Durability Via a Removable Carbon Coating. *ACS Appl. Mater. Interfaces* **2017,** *9*, 31806-31815.

(16) Sandström, R.; Hu, G.; Wågberg, T. Compositional Evaluation of Coreduced Fe–Pt Metal Acetylacetonates as Pem Fuel Cell Cathode Catalyst. *ACS Appl. Energy Mater.* **2018,** *1*, 7106-7115.

(17) Kavita, S.; Reddy, V. R.; Lalla, N. P.; Gupta, A. Evolution of Structural and Magnetic Properties of Fept/C Granular Films with Thermal Annealing. *Solid State Commun.* **2011,** *151*, 794-797.

(18) Chen, L.; Bock, C.; MacDougall, B.; Mercier, P. H. J. Characteristics of Cubic and Tetragonal Ptxfey/C and Ptxfexcu/C Catalysts for the O-2 Electro-Reduction. In *Nanostructured Materials for Energy*

Storage and Conversion, Zaghib, K.; Chiu, W.; Ramani, V.; Liaw, B. Y.; Julien, C.; Mustain, W.; VanSchalkwijk, W., Eds. Electrochemical Soc Inc: Pennington, **2011**, pp 69-80.